

Temperature Steerable Flows and Boltzmann Generators

Manuel Dibak,^{1,*} Leon Klein,^{1,*} Andreas Krämer,¹ and Frank Noé^{1,2,3,4,†}

¹*Department of Mathematics and Computer Science,
Freie Universität Berlin, Arnimallee 12, 14195 Berlin, Germany*

²*Department of Physics, Freie Universität Berlin, Arnimallee 12, 14195 Berlin, Germany*

³*Department of Chemistry, Rice University, Houston, Texas 77005, USA*

⁴*Microsoft Research, Station Road, Cambridge, United Kingdom*

Boltzmann generators approach the sampling problem in many-body physics by combining a normalizing flow and a statistical reweighting method to generate samples in thermodynamic equilibrium. The equilibrium distribution is usually defined by an energy function and a thermodynamic state. Here we propose temperature-steerable flows (TSF) which are able to generate a family of probability densities parametrized by a choosable temperature parameter. TSFs can be embedded in generalized ensemble sampling frameworks to sample a physical system across multiple thermodynamic states.

I. INTRODUCTION

Sampling equilibrium states of many-body systems such as molecules, materials or spin models is one of the grand challenges of statistical physics. Equilibrium densities of system states \mathbf{x} are often given in the form

$$\mu_X(\mathbf{x}) \propto \exp[-u(\mathbf{x})], \quad (1)$$

where $u(\mathbf{x})$ is a reduced (unit-less) energy that combines the system's potential $U(\mathbf{x})$ (if momenta are of interest we have the Hamiltonian energy instead) with thermodynamic variables that define the statistical ensemble. In the canonical ensemble the reduced energy is given by $u(\mathbf{x}) = U(\mathbf{x})/\tau$ where the thermal energy $\tau = k_B T$ is proportional to the temperature T and k_B is the Boltzmann constant. In order to model a system across a range of thermodynamic states, we would like to sample a family of densities parameterized by the thermodynamic control variables – in the canonical ensemble,

$$\mu_X^\tau(\mathbf{x}) \propto \exp\left(-\frac{U(\mathbf{x})}{\tau}\right). \quad (2)$$

The most common approaches to sample densities (1) in physics and chemistry are Markov chain Monte Carlo (MCMC) or molecular dynamics (MD) – both proceed in steps, making small changes to \mathbf{x} at a time, and guarantee that the target density (1) will be sampled asymptotically. The convergence of such sampling algorithms is often slowed down by barriers in the energy landscape, which may result in very long, possibly unfeasible simulation times.

Additionally, many applications require running simulations at various thermodynamic states, e.g., to study the phase behavior and temperature-dependence of materials and biological matter [1, 2]. Moreover, generalized ensemble methods such as parallel tempering (PT) are frequently used to facilitate transitions across energy barriers and thereby enhance sampling. However, these techniques often require dozens of parallel simulations to enable Monte-Carlo exchanges between different temperatures [3, 4].

A novel alternative to traditional sampling methods are generative machine learning models. Recently, there has been a lot of interest in training normalizing flows [5–9] to sample densities of many-body physics systems such as in Eq. (1) directly without having to run long, correlated simulation chains. Normalizing flows (see Appendix A for a brief introduction) transform an easy-to-sample prior distribution $p_Z(\mathbf{z})$, e.g. a multivariate normal distribution, via a transformation $\mathbf{x} = f(\mathbf{z})$ to the output distribution $p_X(\mathbf{x})$. If $f(\mathbf{z})$ is invertible, $p_X(\mathbf{x})$ can be computed by the change of variable formula

$$p_X(\mathbf{x}) = p_Z(\mathbf{z}) |\det J_f(\mathbf{z})|^{-1}. \quad (3)$$

Boltzmann Generators (BGs) [10] combine normalizing flows to minimize the distance between Eqs. (1) and (3) with a statistical reweighting or resampling method to generate unbiased samples from Eq. (1). This and similar approaches have been used to sample configurations of molecular and condensed matter systems [10, 11], spin models [12–14] and gauge configuration in lattice quantum chromodynamics [15–18]. However, these previous generative approaches are only able to sample at a single predefined thermodynamic state.

This letter shows that normalizing flows can be generalized to families of ensembles across multiple temperatures and thereby greatly increase the range of

* These authors contributed equally to this work

† frank.noe@fu-berlin.de; corresponding author

thermodynamic states accessible to a sampling algorithm. Specifically, we develop temperature-steerable flows (TSFs) that correctly parametrize the distribution p_X by a temperature variable τ such that it follows Eq. (2). We evaluate the method on the XY model [19] finding the correct temperature dependence of the magnetization. Moreover we show for two small peptides, alanine dipeptide and tetrapeptide, that the TSF is capable of producing samples close to equilibrium at different temperatures. When trained on a single high temperature, the TSF can simultaneously sample at lower temperatures of interest, allowing a reliable estimation of physical observables and conformational distributions. Finally, due to this property, TSFs are used to facilitate exchanges in classical parallel tempering MD and thereby reduce autocorrelation times significantly.

II. TEMPERATURE-STEERABLE FLOWS

Temperature scaling Up to a normalization constant, a change from temperature τ to τ' corresponds to raising the Boltzmann distribution to the power of $\kappa = \tau/\tau'$, $\mu_X^{\tau'}(\mathbf{x}) \propto [\mu_X^\tau(\mathbf{x})]^\kappa$. We now consider normalizing flows f_τ with priors p_Z^τ that depend on τ as a steerable parameter. Using Eq. (3) the output distribution of a flow scales temperatures equally, if for any two temperatures τ, τ' ,

$$p_Z^{\tau'}(\mathbf{z}) |\det J_{f_{\tau'}}(\mathbf{z})|^{-1} \propto [p_Z^\tau(\mathbf{z}) |\det J_{f_\tau}(\mathbf{z})|^{-1}]^\kappa. \quad (4)$$

In this Letter we thus consider flows to be temperature steerable, if they preserve this scaling condition. We construct flows that preserve this proportionality in two different manners: by either keeping the Jacobian constant and preserving the scaling condition in the prior or selecting a constant prior and respecting the scaling condition in the flow.

A. Temperature steerable flows by volume preservation

The proportionality in the prior distribution can be matched by Gaussians with variance τ , i.e., $p_Z^\tau(\mathbf{z}) = \mathcal{N}(\mathbf{z} | 0, \tau)$, which fulfills $p_Z^{\tau'}(\mathbf{z}) \propto [p_Z^\tau(\mathbf{z})]^\kappa$. This results in a condition on the Jacobian of the flow $|\det J_{f_\tau}(\mathbf{z})|^\kappa \propto |\det J_{f_{\tau'}}(\mathbf{z})|$. Hence, flows with constant Jacobians, i.e. $|\det J_{f_{\tau'}}(\mathbf{z})| = \text{const.}$, are temperature steerable.

This still holds for so-called augmented normalizing flows [21], where the prior and target distributions are augmented with a Gaussian distribution $p_A^\tau(\mathbf{q}) = \mathcal{N}(\mathbf{q} | 0, \tau)$ and $p_A^\tau(\mathbf{p}) = \mathcal{N}(\mathbf{p} | 0, \tau)$ respectively. This augmented flow f_τ is trained to match the output dis-

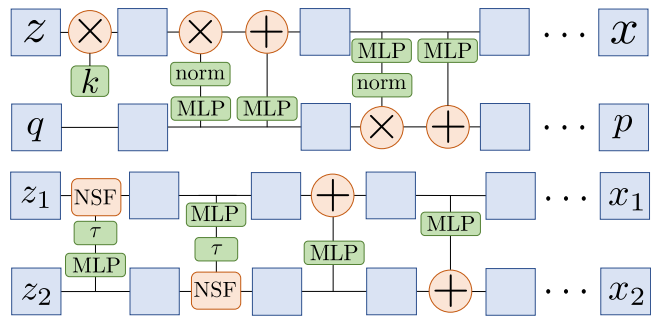


Figure 1. Temperature steerable flow architectures based on coupling layers, which include element-wise multiplication (\times) and addition ($+$). **Top:** Auxiliary momenta \mathbf{q} and coordinates \mathbf{z} are coupled with volume preserving networks where the outputs of the multi-layer perceptron (MLP) used to generate the scaling variables are normalized. The first layer multiplies the latent space coordinates \mathbf{z} with a scalar factor k , which adjusts for the difference in entropy between latent and phase space. **Bottom:** Temperature steerable neural spline flows architecture. Samples from the uniform distribution are split into two channels which are conditioned on the neural spline flows (NSF) transformation of the other channel. The parameters for the flow are transformed to the given temperature τ . This is followed by several layers of volume-preserving transformations [20]. See Appendix A for a description of the flow transformations.

tribution $p_{X,A}^\tau(\mathbf{x}, \mathbf{p})$ with the joint target distribution $\mu_X^\tau(\mathbf{x})p_A^\tau(\mathbf{p})$. The auxiliary variables can be interpreted as physical momenta [9], making the architecture similar to the Hamiltonian Monte Carlo method [22]. However, in contrast we do not propagate the system by Hamiltonian dynamics, but learn a (deterministic) flow, as in Hamiltonian flows [23, 24]. As we are mostly interested in the Boltzmann distribution $\mu_X(\mathbf{x})$ of the positions, this architecture can also be viewed as a stochastic normalizing flow [11].

To generate configuration samples \mathbf{x} from the marginal output distribution $p_X^\tau(\mathbf{x})$ at temperature τ , we follow three consecutive steps: (1) sample the latent configuration $\mathbf{z} \sim p_Z^\tau(\mathbf{z})$ and auxiliary momenta $\mathbf{q} \sim p_A^\tau(\mathbf{q})$, and define the point in phase space (\mathbf{z}, \mathbf{q}) ; (2) propagate the point in phase space by the flow $(\mathbf{x}, \mathbf{p}) = f_\tau(\mathbf{z}, \mathbf{q})$; and (3) project onto the configuration variables \mathbf{x}

An expressive volume-preserving dynamics, i.e. $|\det J_{f_\tau}(\mathbf{z}, \mathbf{q})| = 1$, is obtained by altering real-valued non-volume-preserving transformations [20], such that the product of the outputs of the scaling layers is equal to unity. This is done by subtracting the mean of the log outputs from each scaling layer as in Ref. [25]. In addition to these volume preserving layers we scale the latent space coordinates by a trainable scalar, which al-

lows us to adjust for the entropy difference between the prior and the target. The resulting flow architecture, which still fulfills the scaling condition (4), is shown in Fig. 1 top.

As the flow fulfills the temperature scaling condition, a temperature change of the augmented prior, i.e., $\tau \rightarrow \tau'$, changes the output accordingly. In the case of a factorized output distribution $p_{X,A}^\tau(\mathbf{x}, \mathbf{p}) = p_X^\tau(\mathbf{x})p_A^\tau(\mathbf{p})$, the marginal output distribution $p_X^\tau(\mathbf{x})$ is scaled correctly with the temperature as well. This is ensured if the joint target distribution $\mu_{X,A}^\tau(\mathbf{x}, \mathbf{p}) = \mu_X^\tau(\mathbf{x})p_A^\tau(\mathbf{p})$ is matched correctly.

B. Temperature steerable flows with uniform prior

Instead of a Gaussian prior, one can also use a uniform prior distribution on the unit box $[0, 1]^d$ in combination with a single flow layer that scales with the temperature to construct a TSF. While finding a flow architecture that precisely reproduces the temperature scaling property is difficult, a good approximation is obtained using neural spline flows [26, 27]. With this type of flow we can adjust the parameters given the temperature, such that the temperature scaling is approximately correct (see Appendix B). In addition we combine it with volume preserving flows, i.e. nonlinear independent component estimation (NICE) [28], to obtain a more expressive transformation [see Fig. 1 (bottom)].

C. Training

As in Ref. [10], the flows are trained by a combination of a maximum-likelihood and energy-based loss. Maximum-likelihood training minimizes the negative log likelihood

$$\begin{aligned} \mathcal{L}_{ML} &= \langle -\log p_{X,A}^\tau \rangle_{\mu_{X,A}^\tau} \\ &= \langle -\log p_{Z,A}[f_\tau^{-1}(\mathbf{x}, \mathbf{p})] \\ &\quad - \log \left| \det J_{f_\tau^{-1}}(\mathbf{x}, \mathbf{p}) \right| \rangle_{\mathbf{x}, \mathbf{p} \sim \mu_X^\tau(\mathbf{x})p_A^\tau(\mathbf{p})}, \end{aligned} \quad (5)$$

which agrees with the forward Kullback-Leibler divergence up to a constant. Computing this expectation requires samples from the product distribution $\mu_X^\tau(\mathbf{x})p_A^\tau(\mathbf{p})$, where the configurations \mathbf{x} are generated by (MD) simulations, and momenta \mathbf{p} are independent Gaussian noise.

As the target energy $u(\mathbf{x}, \mathbf{p})$ is defined by the physical system of interest, we can also use energy-based training, which minimizes the reverse Kullback-Leibler

divergence

$$\begin{aligned} \mathcal{L}_{KL} &= \langle -\log \mu_{X,A}^\tau + \log p_{X,A}^\tau \rangle_{p_{X,A}^\tau} \\ &= \langle \tau^{-1} \left(U(\mathbf{x}) + \frac{\|\mathbf{p}\|^2}{2} \right) \\ &\quad - \log |\det J_{f_\tau}(\mathbf{z}, \mathbf{q})| \rangle_{\mathbf{z}, \mathbf{q} \sim p_Z^\tau(\mathbf{z})p_A^\tau(\mathbf{q})} \\ &\quad + \text{const.} \end{aligned} \quad (6)$$

with $(\mathbf{x}, \mathbf{p}) = f_\tau(\mathbf{z}, \mathbf{q})$. This expectation is computed over the thermodynamic ensemble generated by the flow at a given temperature. A TSF trained with Eqs. (5) and (6) will implicitly learn a representation of the Boltzmann distribution that is transferable across temperatures. It can still be useful to combine different target temperatures during training to broaden the range of temperatures at which the TSF performs well.

Furthermore, we can also combine training by example and training by energy [10] using a convex combination $\mathcal{L} = (1 - \lambda)\mathcal{L}_{ML} + \lambda\mathcal{L}_{KL}$.

D. Unbiased sampling: Importance sampling and latent Monte Carlo

As in Ref. [10], we use two different methods to produce unbiased samples from the target distribution μ_X^τ . First, we employ the flow as an importance sampler and compute thermodynamic observables $\langle o \rangle_{\mu_X^\tau}$ by Zwanzig reweighting

$$\langle o \rangle_{\mu_X^\tau} = \frac{\langle o \cdot e^{-U/\tau - \log p_X^\tau} \rangle_{p_X^\tau}}{\langle e^{-U/\tau - \log p_X^\tau} \rangle_{p_X^\tau}}. \quad (7)$$

Second, we extend the flow-based MCMC moves from Ref. [10] to the (augmented) phase space.

A proposal \mathbf{x}' is generated from configuration \mathbf{x} by sampling auxiliary momenta $\mathbf{p} \sim p_A^\tau(\mathbf{p})$, then applying the inverse dynamics $(\mathbf{z}, \mathbf{q}) = f_\tau^{-1}(\mathbf{x}, \mathbf{p})$, followed by a random displacement $(\mathbf{z}', \mathbf{q}') = (\mathbf{z} + \Delta\mathbf{z}, \mathbf{q} + \Delta\mathbf{q})$, with $\Delta\mathbf{z}, \Delta\mathbf{q} \sim \mathcal{N}(0, \sigma^2)$, and finally transforming back $(\mathbf{x}', \mathbf{p}') = f_\tau(\mathbf{z}', \mathbf{q}')$. Accepting such a step with probability

$$\begin{aligned} &p_{\text{acc}}^\tau((\mathbf{x}, \mathbf{p}) \rightarrow (\mathbf{x}', \mathbf{p}')) \\ &= \min \left\{ 1, \exp \left[-\tau^{-1} \left(U(\mathbf{x}') - U(\mathbf{x}) + \frac{\|\mathbf{p}'\|^2}{2} - \frac{\|\mathbf{p}\|^2}{2} \right) \right] \right\} \end{aligned} \quad (8)$$

guarantees detailed balance in configuration space and thus ensures convergence to the Boltzmann distribution. As the TSF is able to generate distributions at several

temperatures, we can combine the MCMC moves with PT [3, 29, 30]. Additionally to TSF-MCMC steps at a set of temperatures, samples can be randomly exchanged between two randomly chosen temperatures with the usual acceptance probability. A summary of the sampling algorithm is given in Appendix C.

III. EXPERIMENTS

We carry out experiments for the XY model and two small peptides, showing that TSFs can sample the respective Boltzmann distributions at different temperatures efficiently. The resulting flows are used to compute observables at low-temperature states from high-temperature simulations and compute temperature-dependent quantities such as absolute free energy from samples at a single thermodynamic state (see Appendix E).

A. XY model

As an example with angular symmetry, we investigate the XY model, which can be considered a continuous state-space version of the Ising model. In our experiments we consider quadratic two dimensional lattices with $N \times N$ spins. Each spin has a continuous angle $\theta_i \in [-\pi; \pi]$ and is represented by $\mathbf{s}_i = (\cos \theta_i, \sin \theta_i)^T$. Each spin interacts with its four nearest neighbors and an external field $\mathbf{h} = (h, 0)$. Hence, the Hamiltonian of the system is given by

$$\mathcal{H}(s_1, \dots, s_{N^2}) = -J \sum_{\langle ij \rangle} \mathbf{s}_i \cdot \mathbf{s}_j - \sum_i \mathbf{h} \cdot \mathbf{s}_i$$

where $\sum_{\langle ij \rangle}$ denotes the sum over all nearest neighbor pairs with periodic boundaries and J is the interaction constant. For our experiments we select the parameters as $J = h = k_B T_0$ and a lattice of 16×16 spins. As observable, we select the mean squared magnetization per spin $\langle M^2 \rangle / N^2 = N^{-2} \langle \sum_i \mathbf{s}_i \cdot \mathbf{s}_i \rangle$ at a given temperature. For producing reference configurations, we use long runs of Glauber dynamics [31]. The TSF consists of a uniform prior, a temperature scaled NSF, followed by seven blocks of circular NICE [see Fig. 1 (bottom) and Appendix F for details]. Training is performed solely with the energy-based loss [Eq. (6)]. Since NSFs are only approximately temperature scaling, we use a convex combination of temperatures $T = \{0.5, 1.0, 1.3\}T_0$ for training. We generate data sets at temperatures ranging $0.5T_0, 0.6T_0, \dots, 1.0T_0$ and observe an excellent overlap of the reweighted energies at the highest and lowest temperature with the reference

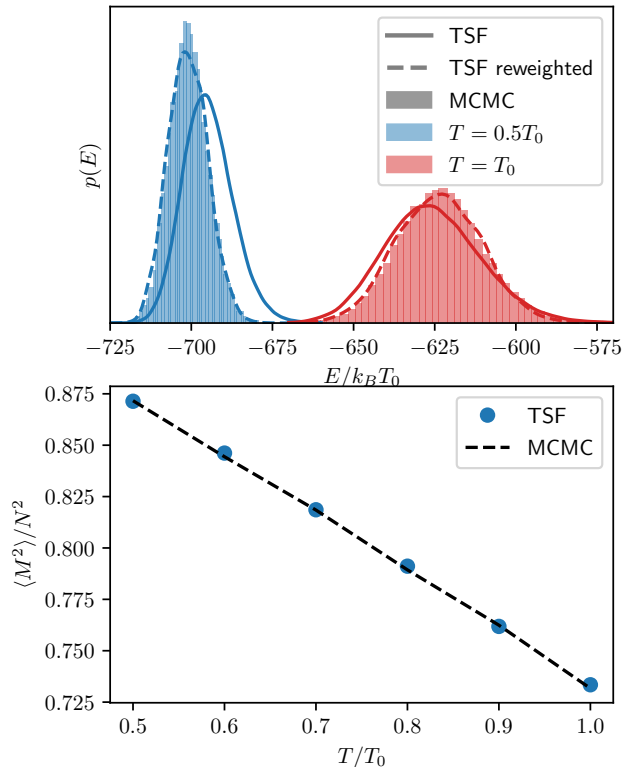


Figure 2. Results of the TSF trained on the two dimensional XY model. **Top:** Distribution of energies at the training temperatures T_0 and $0.5T_0$ obtained by MCMC, TSF and TSF with reweighting. **Bottom:** Magnetization as a function of the temperature compared between the TSF and MCMC samples.

configurations [Fig. 2 (top)]. Furthermore, we compare the mean squared magnetization per spin and again find excellent agreement between TSF and Glauber dynamics [Fig. 2 (bottom)].

B. Alanine di- and tetrapeptide

We further test TSFs on the alanine di- and tetrapeptide molecules in an implicit solvent model. For this system we use an invertible coordinate transformation layer and operate the TSF on a representation of the molecule in terms of distances and angles. Our goal is to use samples at $T = 600$ K to train the TSF and then use the TSF to sample at $T = 300$ K, comparing it to a MD simulation at $T = 300$ K.

Alanine tetrapeptide With the TSF we are able to generate samples at $T = 300$ K that closely resemble the equilibrium distribution. To demonstrate this, we project the configurations into the space of the slowest

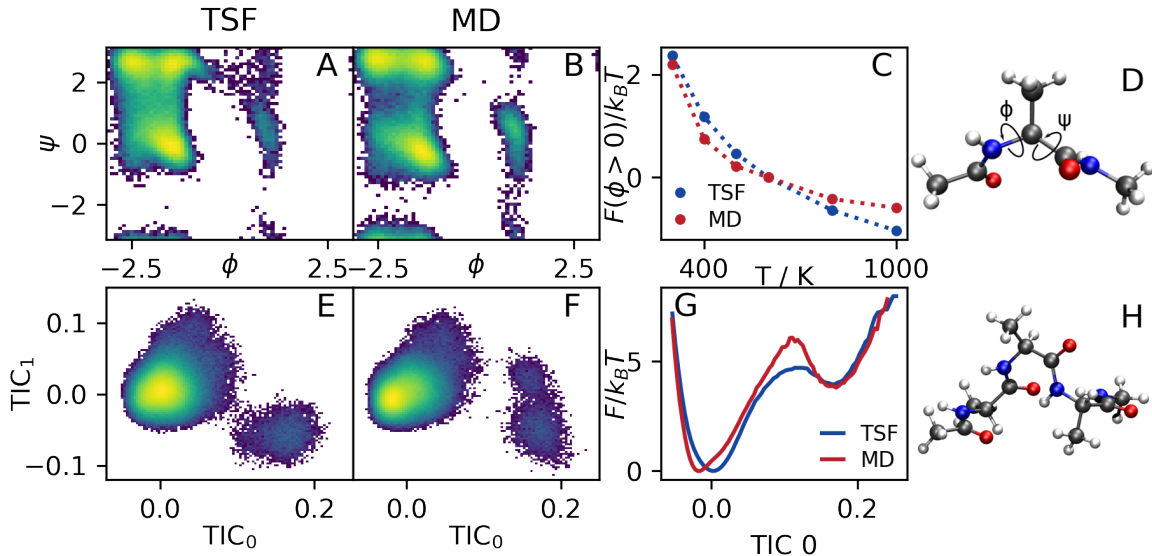


Figure 3. Results for alanine dipeptide (ala2) (**D**, first row) and alanine tetrapeptide (ala4) (**H**, second row) in implicit solvent. All TSFs are trained from samples at 600K **A**, **B**: Ramachandran plots produced by the TSF and MD at 300K. **C**: Comparison of the free energy difference of the two metastable states along the ϕ axis. **E**, **F**: Comparison of the first two time-independent components (TICs) of ala4 at the sampling temperature of 300K. Figure **G** The free energy along the first TIC.

transition between states. These are determined by a time-independent component analysis (TICA [32]) from an exhaustive MD simulation at $T = 300$ K. We observe generally good agreement with MD simulations at the low temperature (Figs. 3 E-G) in the relevant slowest coordinates, while slightly underestimating the barrier height (Fig. 3 G).

Alanine dipeptide We use the TSF to generate samples in configuration space and compare the Ramachandran plots. At $T = 300$ K (Figs. 3 A and B) the TSF still finds the major minima at around $\phi \approx -2$, but under-samples the minimum at $\phi \approx 1$. This deviation from the target distribution likely stems from limited expressivity of the flow. We further utilize the TSF to compare the free energy difference of the two states along the ϕ axis as a function of the temperature (Fig. 3 C). We observe an exact match at the training temperature and slight deviations when moving away from it. To recover the the correct distribution along the ϕ angles, we use the Monte Carlo scheme in a PT fashion with eight temperatures in the range 300-600 K [see Fig. 7 (bottom)].

To assess the efficiency of the sequential sampling procedure, we compare it to the replica exchange molecular dynamics simulation (REMD) at the same temperatures. We observe that for ten independent runs, in REMD only seven transition between the metastable

Table I. Efficiency as the number of effective steps per underlying sampling step for different sampling methods.

Method:	TSF-PT	REMD	MD(600K)	MD(300K)
$\eta \times 10^4$	1.36	0.32	0.38	0.02

states within 10 M steps, while all 10 transition with the TSF-PT method, which additionally only consists of 4M steps [Fig. 4 (top)]. Furthermore, the auto-correlation of the slowest process [Fig. 4 (bottom)], which are the transitions along the ϕ angle, decays considerably faster in the TSF-PT method. In addition, we compare the methods based on their sampling efficiency $\eta = N_{\text{eff}}/N$, where N is the number of underlying MCMC steps and N_{eff} is the effective sample size (see Appendix D for details). Table I shows that the TSF-PT method produces independent samples at about four times the rate of the REMD method.

IV. DISCUSSION

In this Letter, we derived and constructed temperature steerable flows (TSFs) that correctly scale the output distribution of a BG with temperature. To this end we formulated a condition for such flows and intro-

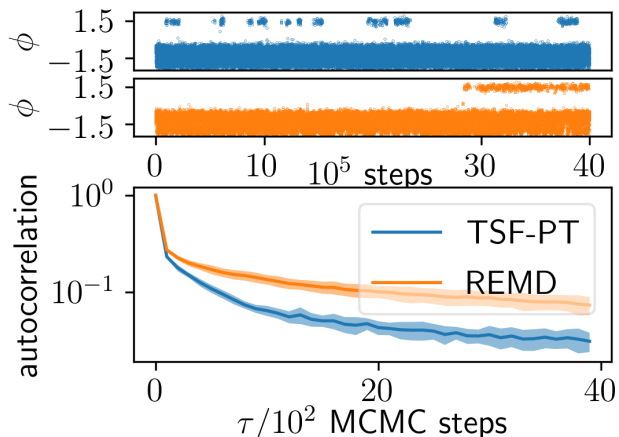


Figure 4. Comparison of replica exchange molecular dynamics simulation (REMD) and the TSF with parallel tempering (TSF-PT), operating in a PT scheme on 8 different temperatures in the range between 300 and 600 K **Top:** One example trajectory of ϕ angles of the 10 independent runs. Despite being over two times longer, no transitions are observed in three out of the ten REMD runs, while all of the TSF-PT trajectories cross many times between the two metastable states. **Bottom:** Autocorrelation of the ϕ angle as a function of underlying MCMC/MD steps. The autocorrelation function decays more rapidly in the TSF-PT method. This hints toward this method being more sampling efficient. Non traversing trajectories of the REMD method were excluded in the calculation of the autocorrelation.

duced two different methods of constructing them. We showed that this type of flow can be used to train a BG at one temperature and generate distributions at lower temperatures.

For the XY model we were able to predict the correct temperature dependence of the magnetization. Furthermore, we showed for alanine dipeptide that the efficiency of parallel tempering can be improved by using our TSF for the MCMC proposals at different temperatures. Further progress could be made by combining samples at different temperatures when collecting training data and thus improve the quality of the BG.

While the presented results demonstrate the promise and uniqueness of the TSF method, practical applications to high-dimensional physical systems of interest will likely require further modifications to the network architecture. Future work should consider combining TSF with conditioner networks that respect the symmetries of the potential energy. In this spirit, the presented temperature-scaling property complements existing equivariant flows that maintain group transformations such as rotation and permutation [33–36].

ACKNOWLEDGMENTS

V. ACKNOWLEDGMENT

We gratefully acknowledge support by the Deutsche Forschungsgemeinschaft (SFB1114, Projects No. C03, No. A04, and No. B08), the European Research Council (ERC CoG 772230 “ScaleCell”), the Berlin Mathematics center MATH+ (AA1-6), and the German Ministry for Education and Research (BIFOLD - Berlin Institute for the Foundations of Learning and Data). We thank Jonas Köhler, Michele Invernizzi, and Yaoyi Chen for insightful discussions. Moreover, we thank the anonymous reviewers for their constructive feedback.

-
- [1] M Böttcher, S Heinze, S Egorov, J Sinova, and B Dupé. B-t phase diagram of pd/fe/ir(111) computed with parallel tempering monte carlo. *New Journal of Physics*, 20(10):103014, oct 2018.
- [2] René Wuttke, Hagen Hofmann, Daniel Nettels, Madeleine B. Borgia, Jeetain Mittal, Robert B. Best, and Benjamin Schuler. Temperature-dependent solvation modulates the dimensions of disordered proteins. *Proceedings of the National Academy of Sciences*, 111(14):5213–5218, 2014.
- [3] Robert H Swendsen and Jian-Sheng Wang. Replica monte carlo simulation of spin-glasses. *Physical review letters*, 57(21):2607, 1986.
- [4] David J. Earl and Michael W. Deem. Parallel tempering: Theory, applications, and new perspectives. *Phys. Chem. Chem. Phys.*, 7:3910–3916, 2005.
- [5] Esteban G. Tabak and Eric Vanden-Eijnden. Density estimation by dual ascent of the log-likelihood. *Commun. Math. Sci.*, 8:217–233, 2010.
- [6] Danilo Rezende and Shakir Mohamed. Variational inference with normalizing flows. In *International conference on machine learning*, pages 1530–1538. PMLR, 2015.
- [7] George Papamakarios, Eric Nalisnick, Danilo Jimenez Rezende, Shakir Mohamed, and Balaji Lakshminarayanan. Normalizing flows for probabilistic modeling and inference. *Journal of Machine Learning Research*, 22(57):1–64, 2021.
- [8] Ivan Kobyzev, Simon Prince, and Marcus Brubaker. Normalizing flows: An introduction and review of current methods. *IEEE Transactions on Pattern Analysis and Machine Intelligence*, 2020.
- [9] Shuo-Hui Li, Chen-Xiao Dong, Linfeng Zhang, and Lei Wang. Neural canonical transformation with symplectic flows. *Physical Review X*, 10(2):021020, 2020.
- [10] Frank Noé, Simon Olsson, Jonas Köhler, and Hao Wu. Boltzmann generators-sampling equilibrium states of many-body systems with deep learning. *Science*, 365:eaaw1147, 2019.
- [11] Hao Wu, Jonas Köhler, and Frank Noé. Stochastic normalizing flows. *Advances in Neural Information Processing Systems*, 33:5933–5944, 2020.
- [12] S. Li and Lei Wang. Neural network renormalization group. *Physical review letters*, 121 26:260601, 2018.
- [13] Kim A. Nicoli, Shinichi Nakajima, Nils Strodthoff, W. Samek, K. Müller, and P. Kessel. Asymptotically unbiased estimation of physical observables with neural samplers. *Physical review. E*, 101 2-1:023304, 2020.
- [14] Kim A Nicoli, Christopher J Anders, Lena Funcke, Tobias Hartung, Karl Jansen, Pan Kessel, Shinichi Nakajima, and Paolo Stornati. Estimation of thermodynamic observables in lattice field theories with deep generative models. *Physical review letters*, 126(3):032001, 2021.
- [15] MS Albergo, G Kanwar, and PE Shanahan. Flow-based generative models for markov chain monte carlo in lattice field theory. *Physical Review D*, 100(3):034515, 2019.
- [16] Denis Boyda, Gurtej Kanwar, Sébastien Racanière, Danilo Jimenez Rezende, Michael S Albergo, Kyle Cranmer, Daniel C Hackett, and Phiala E Shanahan. Sampling using su (n) gauge equivariant flows. *Physical Review D*, 103(7):074504, 2021.
- [17] Gurtej Kanwar, Michael S Albergo, Denis Boyda, Kyle Cranmer, Daniel C Hackett, Sébastien Racanière, Danilo Jimenez Rezende, and Phiala E Shanahan. Equivariant flow-based sampling for lattice gauge theory. *Physical Review Letters*, 125(12):121601, 2020.
- [18] Michael S Albergo, Gurtej Kanwar, Sébastien Racanière, Danilo J Rezende, Julian M Urban, Denis Boyda, Kyle Cranmer, Daniel C Hackett, and Phiala E Shanahan. Flow-based sampling for fermionic lattice field theories. *Physical Review D*, 104(11):114507, 2021.
- [19] H. E. Stanley. Dependence of critical properties on dimensionality of spins. *Phys. Rev. Lett.*, 20:589–592, Mar 1968.
- [20] Laurent Dinh, Jascha Sohl-Dickstein, and Samy Bengio. Density estimation using real nvp. *arXiv preprint arXiv:1605.08803*, 2016.
- [21] C. Huang, Laurent Dinh, and Aaron C. Courville. Augmented normalizing flows: Bridging the gap between generative flows and latent variable models. *ArXiv*, abs/2002.07101, 2020.
- [22] Simon Duane, Anthony D Kennedy, Brian J Pendleton, and Duncan Roweth. Hybrid monte carlo. *Physics letters B*, 195(2):216–222, 1987.
- [23] Samuel Greydanus, Misko Dzamba, and Jason Yosinski. Hamiltonian neural networks. In *Advances in Neural Information Processing Systems*, pages 15379–15389, 2019.
- [24] Peter Toth, Danilo Jimenez Rezende, Andrew Jaegle, Sébastien Racanière, Aleksandar Botev, and Irina Higgins. Hamiltonian generative networks. *ArXiv*, abs/1909.13789, 2019.
- [25] P. Sorrenson, C. Rother, and U. Köthe. Disentanglement by nonlinear ICA with general incompressible-flow networks (GIN). *ArXiv*, abs/2001.04872, 2020.
- [26] Conor Durkan, Artur Bekasov, Iain Murray, and George Papamakarios. Neural spline flows. *Advances in neural information processing systems*, 32, 2019.
- [27] Danilo Jimenez Rezende, George Papamakarios, Sébastien Racanière, Michael Albergo, Gurtej Kanwar, Phiala Shanahan, and Kyle Cranmer. Normalizing flows on tori and spheres. In Hal Daumé III and Aarti Singh, editors, *Proceedings of the 37th International Conference on Machine Learning*, volume 119 of *Proceedings of Machine Learning Research*, pages 8083–8092. PMLR, 13–18 Jul 2020.
- [28] L. Dinh, D. Krueger, and Y. Bengio. Nice: Nonlinear independent components estimation. *arXiv:1410.8516*, 2015.
- [29] Charles J. Geyer. Markov chain monte carlo maximum likelihood. In *Proceedings of the 23rd Symposium on the Interface*, pages 156–163, 1991.

- [30] K. Hukushima and K. Nemoto. Exchange monte carlo method and application to spin glass simulations. *Journal of the Physical Society of Japan*, 65:1604–1608, 1996.
- [31] Roy J Glauber. Time-dependent statistics of the ising model. *Journal of mathematical physics*, 4(2):294–307, 1963.
- [32] Guillermo Pérez-Hernández, Fabian Paul, Toni Giorgino, Gianni De Fabritiis, and Frank Noé. Identification of slow molecular order parameters for markov model construction. *The Journal of chemical physics*, 139(1):07B604_1, 2013.
- [33] Jonas Köhler, Leon Klein, and Frank Noé. Equivariant flows: exact likelihood generative learning for symmetric densities. In *International Conference on Machine Learning*, pages 5361–5370. PMLR, 2020.
- [34] Danilo Jimenez Rezende, Sébastien Racanière, Irina Higgins, and Peter Toth. Equivariant hamiltonian flows. *arXiv preprint arXiv:1909.13739*, 2019.
- [35] Linfeng Zhang, Lei Wang, et al. Monge-Ampère flow for generative modeling. *arXiv preprint arXiv:1809.10188*, 2018.
- [36] Victor Garcia Satorras, Emiel Hoogeboom, Fabian Fuchs, Ingmar Posner, and Max Welling. E(n) equivariant normalizing flows. In M. Ranzato, A. Beygelzimer, Y. Dauphin, P.S. Liang, and J. Wortman Vaughan, editors, *Advances in Neural Information Processing Systems*, volume 34, pages 4181–4192. Curran Associates, Inc., 2021.
- [37] Esteban G Tabak and Cristina V Turner. A family of nonparametric density estimation algorithms. *Communications on Pure and Applied Mathematics*, 66:145–164, 2013.
- [38] Jan-Hendrik Prinz, Hao Wu, Marco Sarich, Bettina Keller, Martin Senne, Martin Held, John D Chodera, Christof Schütte, and Frank Noé. Markov models of molecular kinetics: Generation and validation. *The Journal of chemical physics*, 134(17):174105, 2011.
- [39] Jun S Liu. *Monte Carlo strategies in scientific computing*. Springer Science & Business Media, 2008.
- [40] Peter Eastman, Jason Swails, John D Chodera, Robert T McGibbon, Yutong Zhao, Kyle A Beauchamp, Lee-Ping Wang, Andrew C Simmonett, Matthew P Harrigan, Chaya D Stern, Rafal P Wiewiora, Bernard R Brooks, and Vijay S Pande. Openmm 7: Rapid development of high performance algorithms for molecular dynamics. *PLOS Computational Biology*, 13:e1005659, 7 2017.
- [41] Kresten Lindorff-Larsen, Stefano Piana, Kim Palmo, Paul Maragakis, John L. Klepeis, Ron O. Dror, and David E. Shaw. Improved side-chain torsion potentials for the amber ff99sb protein force field. *Proteins: Structure, Function, and Bioinformatics*, 78:1950–1958, 6 2010.
- [42] Moritz Hoffmann, Martin Scherer, Tim Hempel, Andreas Mardt, Brian de Silva, Brooke E Husic, Stefan Klus, Hao Wu, Nathan Kutz, Steven L Brunton, and Frank Noé. Deeptime: a python library for machine learning dynamical models from time series data. *Machine Learning: Science and Technology*, 3:015009, 3 2022.

Appendix A: Normalizing flows (NICE and NSF)

Normalizing flows [5, 7, 37] are invertible neural networks f that operate as density maps on top of a prior distribution p_X . They are usually designed such that the following numerical operations are computationally efficient:

- forward evaluation $\mathbf{x} = f(\mathbf{z})$
- inverse evaluation $\mathbf{z} = f^{-1}(\mathbf{x})$,
- evaluation of the Jacobian determinant $|\det J_f(\mathbf{z})|$ and, by extension, its inverse $|\det J_{f^{-1}}(\mathbf{x})|$, and
- computation of the following parameter gradients for training (“backward evaluation”)

$$\nabla_{\theta} f, \nabla_{\theta} f^{-1}, \nabla_{\theta} |\det J_f|, \nabla_{\theta} |\det J_{f^{-1}}|.$$

An important network architecture that meets these requirements are coupling layers, which are algorithmically similar to reversible integrators. They operate on two input vectors (e.g. positions \mathbf{z} and momenta \mathbf{q}), where only one input (e.g. positions) is transformed by an element-wise transform $\mathbf{x} = s(\mathbf{z}; \boldsymbol{\vartheta})$. The transform s is a function that has cheap derivatives and inverse. NICE [20] corresponds to s being a simple sum $s(\mathbf{z}; \boldsymbol{\vartheta}) = \mathbf{z} + \boldsymbol{\vartheta}$. Neural spline flows (NSF) [26] correspond to s being strictly increasing rational quadratic splines, where $\boldsymbol{\vartheta}$ contains the spline knots and slopes (see below).

Crucially, the transform parameters $\boldsymbol{\vartheta}$ are generated by a separate neural network, $\boldsymbol{\vartheta} = c(\mathbf{q}; \boldsymbol{\theta})$. This conditioner network c need not be invertible and can be a simple multilayer perceptron. The term coupling layer denotes the overall trainable transformation

$$\begin{pmatrix} \mathbf{z} \\ \mathbf{q} \end{pmatrix} \mapsto \begin{pmatrix} \mathbf{x} \\ \mathbf{p} \end{pmatrix} = \begin{pmatrix} s(\mathbf{z}; c(\mathbf{q}; \boldsymbol{\theta})) \\ \mathbf{q} \end{pmatrix},$$

which allows efficient inversion and computation of the Jacobian determinant. Stacking such coupling layers and reversing the roles of \mathbf{q}/\mathbf{p} and \mathbf{z}/\mathbf{x} in between yields invertible neural networks that can express complicated diffeomorphisms.

Appendix B: Temperature steerable spline flows

In a spline flow transformation, each element of the input vector is transformed via an invertible scalar function $y_i = F(x_i)$ defined on the unit interval $F : [0, 1] \rightarrow [0, 1]$, s.t. $F(0) = 0$ and $F(1) = 1$. Neural Spline Flows are especially useful when transforming a quantity with circular symmetry as they can easily be adjusted to satisfy the periodicity of the variables. For this transformation to be invertible, it needs to be monotonous. It can

be interpreted as the cumulative distribution function corresponding of a probability density function p defined on the unit interval. The function $F(x)$ is approximated by a spline $s(x)$, a piecewise defined function, which is invertible in each interval. The spline is parametrized by K coordinates, and slopes $(x^{(i)}, y^{(i)}, \delta^{(i)})$ which are the function values and derivatives of $y^{(i)} = F(x^{(i)})$, $\delta^{(i)} = p(x^{(i)})$. The spline then interpolates the function values in between these coordinates. There exists a whole range of different ways to define a spline. The recently proposed Neural Spline Flows (NSF) [26] use quadratic rational splines and have been shown to perform best in a series of tasks. Thus these have been utilized in this work.

A quadratic rational spline can alternatively be defined by N bin widths, heights and slopes (w_i, h_i, δ_i) , with $\sum_i w_i = 1$, $\sum_i h_i = 1$. Assuming that the spline is an approximation of $F(x)$, we find that $h_i = \int_{x_i}^{x_i+w_i} p(x) dx$, with $x_i = \sum_{j=1}^{i-1} w_j$. For the temperature scaling to hold, we assume that $p(x)$ is of the form $p(x) = \exp(\beta v(x))$ for some continuous function $v(x)$. We then see that $\delta_i = \exp(\beta v_i)$, with $v_i = v(x_i)$ and can approximate by the mean value theorem $h_i = \int_{x_i}^{x_i+w_i} p(x) dx \approx \exp(\beta \tilde{v}_i) w_i$, with $\tilde{v}_i = v(\xi)$ for $\xi \in [x_i, x_{i+1}]$. With these assumptions it is clear how

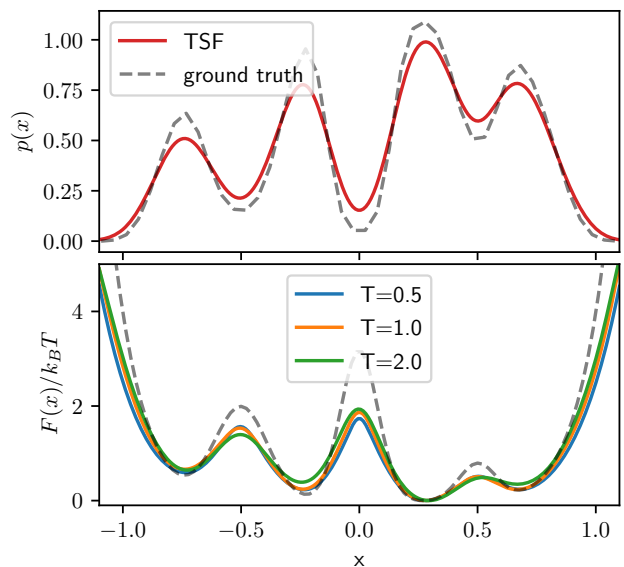


Figure 5. Temperature steerable spline flow as a trained inverse sampler for 1D densities. The free energies are given in units of $k_B T$. In these units the ground truth coincides for different temperatures. The top two figures show an application to the asymmetric double well potential and the bottom two to the Prinz potential [38].

scale the spline parameters to other temperatures

$$h_i^\tau = \exp(\tau \tilde{v}_i) w_i / \sum_i \exp(\tau \tilde{v}_i) w_i,$$

$$\delta_i^\tau = \exp(\tau v_i).$$

Thus the transformation is fully parametrized by the set of values (w_i, v_i, \tilde{v}_i) . To demonstrate that this indeed produces a temperature steering transformation of the variable \mathbf{x} , we apply this method to a test system, namely the Prinz potential [38]. Here we only consider one transformation with fixed weights. We train the set of parameters directly by the KL-loss. We generally observe a good fit to the ground truth (Fig. 5). The temperature steering property is evident by observing, that the free energy almost coincides at the three different temperatures, when expressed in terms of thermal energy.

For higher dimensional systems one makes use of coupling layers. For the temperature scaling condition to hold, we can only use one coupling layer on each subset of coordinates. To further enable the transformation to capture correlations in the system, we combine the procedure with volume preserving transformations.

Appendix C: Sequential sampling algorithm

The TSF-PT algorithm is shown in Algorithm 1. For a random swap of temperatures between two samples \mathbf{x}_i and \mathbf{x}_j at temperatures τ_i and τ_j , detailed balance is preserved by the acceptance probability

$$p_{\text{acc}} = \min \left\{ 1, \exp \left[(U(\mathbf{x}_i) - U(\mathbf{x}_j)) \left(\frac{1}{\tau_i} - \frac{1}{\tau_j} \right) \right] \right\}. \quad (\text{C1})$$

Appendix D: Autocorrelation analysis of Ala 2 runs

Following Liu [39], the effective sample size of an MCMC sampler can be quantified as $N_{\text{eff}} = N/2\tau$ where N is the number of samples and τ denotes the integrated autocorrelation time $\tau = \frac{1}{2} + \sum_{i=1}^{\infty} \rho_i$, with the autocorrelation function (acf) $\rho_i = \text{var}(o(\mathbf{x}^{(0)}), o(\mathbf{x}^{(i)}))$ of some observable o that is chosen to be the slowest process in the system. For the Ala2 system we consider sampling along the ϕ angle to be the slowest process. We define the efficiency of a multi ensemble sampler (e.g. parallel tempering) simultaneously operating at M copies of the system as $\eta = N_{\text{eff}}/N = \frac{1}{2M\tau}$ which quantifies the number of effective (i.e. uncorrelated) samples per underlying sampling step. We specifically compare REMD

```

input :  $l_s = []$  : empty list for samples
          $\tau$  : list of  $N_T$  temperatures
         state  $\leftarrow$  init state :  $N_T$  initial configurations
          $N_{\text{iterations}}$  : number of generated samples
          $n_{\text{propagate}}$  : number of propagation steps
          $n_{\text{swap}}$  : number of temperature swaps

for  $i \leftarrow 1$  to  $N_{\text{iterations}}$  do
  for  $j \leftarrow 1$  to  $n_{\text{propagate}}$  do
    for  $k \leftarrow 1$  to  $N_T$  do
       $\mathbf{x} \leftarrow \text{state}_k$ 
       $\mathbf{p} \leftarrow \text{sample from } p_A^{\tau_k}$ 
       $(\mathbf{z}, \mathbf{q}) \leftarrow D^{-1}((\mathbf{x}, \mathbf{p}))$ 
       $\boldsymbol{\omega} \leftarrow \text{sample from } \mathcal{N}(0, \sigma^2)$ 
       $(\mathbf{z}', \mathbf{q}') \leftarrow (\mathbf{z}, \mathbf{q}) + \boldsymbol{\omega}$ 
       $(\mathbf{x}', \mathbf{p}') \leftarrow D((\mathbf{z}', \mathbf{q}'))$ 
       $p_{\text{acc}} \leftarrow p_{\text{acc}}^{\tau_k}((\mathbf{x}, \mathbf{p}) \rightarrow (\mathbf{x}', \mathbf{p}'))$  (Eq. 8)
      if  $r \sim \mathcal{U}(0, 1) < p_{\text{acc}}$  then
        |  $\text{state}_k \leftarrow \mathbf{x}'$ 
      end
    end
  end
  while  $j < n_{\text{swap}}$  do
    randomly select  $\alpha, \beta \leq N_T, \alpha \neq \beta$ 
     $\mathbf{x} \leftarrow \text{state}_\alpha$ 
     $\mathbf{y} \leftarrow \text{state}_\beta$ 
     $p_{\text{acc}} \leftarrow p_{\text{acc}}(\mathbf{x}, \mathbf{y}, \tau_\alpha, \tau_\beta)$  (Eq. C1)
    if  $r \sim \mathcal{U}(0, 1) < p_{\text{acc}}$  then
      |  $\text{state}_\alpha \leftarrow \mathbf{y}$ 
      |  $\text{state}_\beta \leftarrow \mathbf{x}$ 
    end
  end
  end
   $l_s.\text{append}(\mathbf{x})$ 
   $i \leftarrow i + 1$ 
end

```

output: list of samples l_s
Algorithm 1: Sampling algorithm used in the parallel tempering Ala2 system.

to TSF-PT at 8 different temperatures in the range of 300 K to 600 K for 10 independent runs. Trace plots of the ϕ angles at the lowest temperature 300 K, as well as the acf, are shown in Fig. 6. From Fig. 3 we observe, that the system exhibits two metastable states along this angle. We observe that transitions between these states happen more frequent in TSF-PT method. Despite being twice as long, we observe no transitions between the metastable states for three of the ten independent runs with the REMD method, while all independent runs transition with TSF-PT. This is also reflected in the autocorrelation times, which are considerably lower for the TSF-PT method.

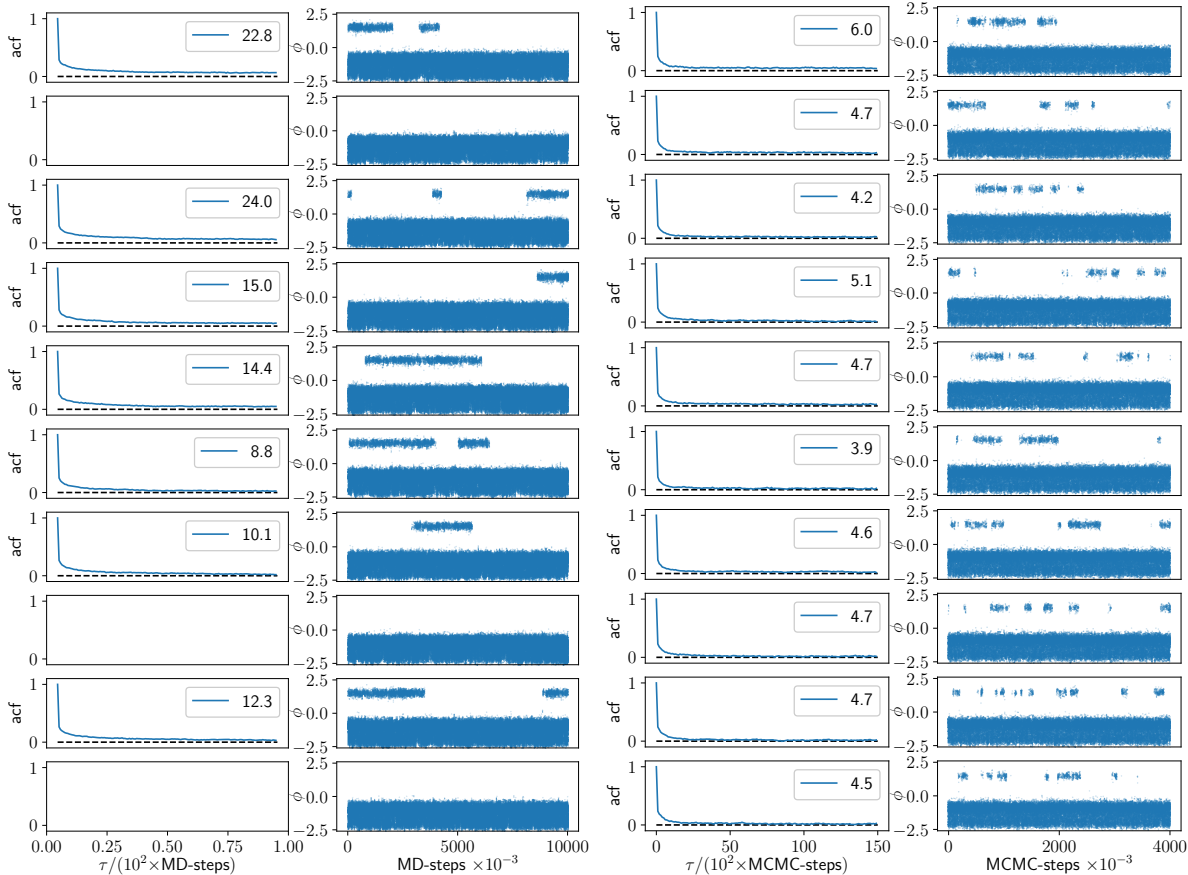


Figure 6. Trace plots and autocorrelation of the ϕ angle in the sampling runs of the Ala2 molecule at $T = 300$ K. Left for replica exchange molecular dynamics (REMD), right for TSF-PT. The numbers in the legends of the autocorrelation function (acf) plots are the integrated autocorrelation times τ . We observe more frequent transitions between the metastable states at $\phi < 0$ and $\phi > 0$ in the TSF-PT method. This is also reflected in the integrated autocorrelation times, which are considerably lower for TSF-PT.

Appendix E: Free energy computation

Using the TSF framework, we are able to compute absolute free energies of a system at different temperatures. The free energy F is given by

$$F = -\tau \ln(Z_\tau), \quad (\text{E1})$$

where $Z_\tau = \int \exp\left(-\frac{U(\mathbf{x})}{\tau}\right) dx^{3N}$ is the partition function. The output distribution $p_X^\tau(\mathbf{x})$ of a normalizing flow is normalized, i.e. $\int p_X^\tau(\mathbf{x}) dx^{3N} = 1$. The energy of the output distribution is given by $u_X^\tau(\mathbf{x}) := -\log p_X^\tau(\mathbf{x})$ and, hence, $p_X^\tau(\mathbf{x}) = \exp(-u^\tau)$. We can use samples from the flow to estimate the partition function and therefore the free energy at a given temperature with a

TSF.

$$\begin{aligned} Z_\tau &= \int e^{-\frac{U(\mathbf{x})}{\tau}} dx^{3N} \\ &= \int e^{-\frac{U(\mathbf{x})}{\tau} + u_X^\tau(\mathbf{x}) - u_X^\tau(\mathbf{x})} dx^{3N} \\ &= \mathbb{E}_{\mathbf{x} \sim p_X^\tau(\mathbf{x})} e^{-\left(\frac{U(\mathbf{x})}{\tau} - u_X^\tau(\mathbf{x})\right)} \end{aligned}$$

where the last step holds, because the output distribution of the flow is normalized. As we can sample with the flow and have access to the target energy $U(\mathbf{x})$ as well as the flow energy $u_D^\tau(\mathbf{x})$, we can compute absolute free energies with the TSF. We show this for a simple four dimensional test system, where it is easy to compute the total free energy. The target is given by a double well potential and the other dimensions are given by standard Normal distributions. A TSF is trained with the ML-loss objective at temperature $\tau = 1$. We see

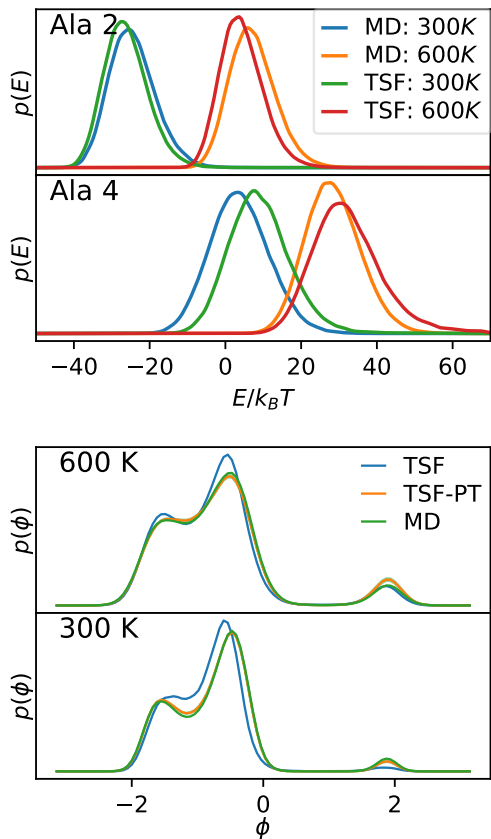


Figure 7. **Top:** Comparison of histograms of configurational energy between samples generated by the TSF and samples generated by MD. **Bottom:** Distribution of the slowest timescale in the Ala 2 system generated by different sampling methods involving the TSF.

good agreement of the free energy computed using the TSF with the ground truth (see Fig. 8). The ground truth is computed with numerical integration.

Appendix F: Detailed description of the systems and networks

Table II. Setup of alanine dipeptide in implicit solvent

Force Fields	Amber ff99SB-ILDN Amber ff99-OBC
Number Atoms	22
Total simulation time 600K	10 ns
Total simulation time 300K	1 ms
PT temperatures [K]	300.0, 331.2, 365.7, 403.8, 445.8, 492.2, 543.4, 600.0

Table III. Network parameters for the different systems under consideration

System	parameters	coupling blocks	training iterations
Ala2	1.9 M	50	3×10^4
Ala4	3.3 M	30	3×10^4
Prinz	30	1	1×10^4
XY-model	8.5 M	7	1×10^3

All experiments were performed on a standard desktop machine equipped with a *Nvidia GeForce 1080 Ti*, on which one training iteration of the Ala 4 system takes around 0.24 seconds. The code will be available at <https://github.com/noegroup/bgflow>.

Alanine dipeptide and alanine tetrapeptide were simulated in OpenMM 7.5 [40] using a Generalized Born implicit solvent model, the Amber ff99SB-ILDN force field [41], and a Langevin integrator with 2 fs time step and 1/ps friction coefficient. The time-lagged independent component analysis (TICA) for alanine tetrapeptide was performed using deeptime [42]. The TICA lag time was chosen as 5 ns based on a subsequent Markov State Model analysis.

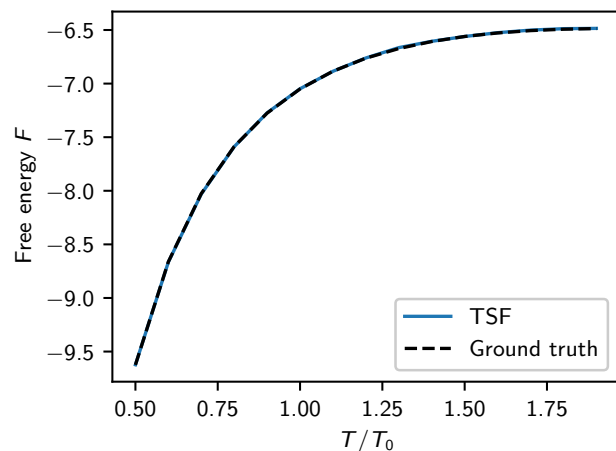


Figure 8. Free energy dependence on the temperature for a four dimensional system computed with a TSF trained at T_0 .